Discover Environment

Case Study

Particulate matter (pm10) monitoring in the United Arab Emirates using a satellite remote sensing based model

Aisha Al Suwaidi[1] · Tarig Ali[1] · Serter Atabay[1] · Mohamed Singer[1] · Ahmed Elaksher[2]

Received: 21 February 2024 / Accepted: 12 April 2024
Published online: 14 May 2024

Abstract
Particulate matter (PM) is one of the major factors causing air pollution, which is considered a concern for human health. Hence, measuring and monitoring the concentrations of these particles is essential. In this study, the main objective is to develop a remote sensing based PM10 monitoring model for the United Arab Emirates (UAE) using Landsat 8 imagery. Landsat 8 images acquired during the four-year period from 2016 to 2022 were obtained and used along with PM10 data collected at 41 ground monitoring stations corresponding to the acquisition of the satellite data (data from 30 stations used for model development 11 stations were used for model testing). The Landsat 8 data was obtained from the United States Geological Survey (USGS) Core Science Systems in the form of Digital Numbers (DNs). The DNs of the four optical bands of Landsat 8 were then converted to top of the atmosphere reflectance (TOA) through radiometric processing, and then used to estimate the Aerosol Optical Thickness. A spectral PM10 model was then developed through regression analysis, correlating AOT to PM10 values obtained at the ground stations. The model provided an R-squared value of 65% and a Root Mean Square Error (RMSE) of 12.55 µg/m3. The results suggest that the developed model is robust in estimating PM10 values and can therefore be used for satellite-based monitoring at any location in the UAE.

Keywords Air quality · Particulate matter · Landsat 8 · Digital numbers · TOA · Satellite remote sensing

1 Introduction

Air quality is an important indicator of human health and wellbeing. Any increases in the concentration of harmful air pollutants can significantly impact human health, increasing risks of cardiovascular diseases, asthma, and premature deaths. Air pollution is one of the most significant environmental issues that are concentrated in urban cities and poses a significant risk to contemporary society, especially with rapid urbanization, industrialization and migration [1] and [2]. Anthropogenic stressors negatively impact the environment such as polluting the air, the water resources and the soil for different plant species [3]. Most air pollution results from the production and use of energy and emissions from factories, power plants, and automobiles [4]. Air pollution whether indoor or outdoor is responsible for approximately 2 million premature deaths and kills around 7 million people a year globally [5] and [6]. Air pollution increases the risks of respiratory and cardiovascular diseases, hospitalizations, which affect the overall economy of the country [7] and [8]. It is evident that people living in environments with poor air quality are more vulnerable to asthma, ventricular hypertrophy, lung cancer, retinopathy, fatal growth, Alzheimer's, and Parkinson's disease. In China, polluted air was responsible

✉ Ahmed Elaksher, elaksher@nmsu.edu | [1]Civil Engineering Department, American University of Sharjah, Sharjah, United Arab Emirates. [2]College of Engineering, New Mexico State University, Las Cruces, USA.

for about 1.2 million deaths in 2010 and around 1.6 million deaths in 2014 [9]. Research has shown that air pollution is a contributing factor to high infant mortality rates in developing nations in Africa [10].

In the context of air pollution, particulate matter (also known as atmospheric aerosols) are fine suspended particles in the form of solid or liquid state and they derive from natural sources such as forest fires, volcanic eruption, desert dust or from human-related activities such as biomass or fossil fuels burning [11]. The concentration of PM is known to be high in regions with increased industrial activity, urbanization, traffic, and with poor emission control measures [12]. These particles have a strong interaction with solar radiation, the temperature, vertical profile, earth surface characteristics, and other thermodynamic variables [12]. Aerosols have different effects on human health, climate dynamics, and visibility [13]. The presence of atmospheric aerosols (PM) in high concentrations in the atmosphere compromises the quality of air and contributes to the rising rates of pollution [14].

The two major types of PM are PM2.5 and PM10, where PM2.5 corresponds to a diameter less than 2.5 μm (fine particles) and PM10 that has a diameter of 10 μm and is classified as coarse particles [15]. Given that the size of PM is very small, those particles can easily enter the human lungs through inhalation and cause huge health risks [16]. Absorption and scattering of solar radiation by these particles can cause serious problems for human health [17] and [18]. Indoor air pollution that results from physical and biological aerosols produced from cooking activities, incenses and air conditioners is a leading cause of pneumonia, stroke, IHD, COPD, and cancer that is linked to 4.5 million annual deaths globally [19] and [20]. A study found an association between air pollution and high levels of PM and human health in UAE, specifically serious diseases such as cardiovascular diseases, cancers, and pulmonary inflammation [21].

Aerosol optical depth (AOD) or Aerosol optical thickness (AOT) is a parameter that provides an estimation of aerosol particles in the air from ground based measurements [22]. The status of the air can be indicated based on the AOD value. Low AOD values indicate that the sky is clear and pure, and higher values mean lower in air visibility and purity due to the presence of aerosols [23]. AOD describes the attenuation of solar radiation in the atmosphere as it gets scattered and/or absorbed by the PM [24]. Monitoring of the AOD by satellite remote sensing is widely used along with ground-based in situ measurements corresponding to the satellite data, provided that satellite imagery provides larger spatial coverage [25]. There is a global ground network of air pollution monitoring stations such as Aerosol Robotic Network (AERONET), which assists in tracking the level of PM concentration and its impact on the globe [26]. AERONET is a ground network that measures many parameters of the atmospheric aerosol robotically, including PM10, and performs data processing and data calibration before providing the data [27]. There are local monitoring stations established in different countries in order to complement and densify global networks [28].

Ground monitoring stations measure air quality accurately, at any time, and are good measuring tools for gauging air pollution levels and trends. However, most ground stations are sparsely distributed and are located near cities limiting the effectiveness and representativeness [29]. The information is limited to the region without incorporation of other influencing factors such as meteorological data, land use categories, sources of emission data, topographic, and socioeconomic factors [30]. Given the limitation of ground monitoring stations, satellite remote sensing-based methods have become very popular. Satellite remote sensors are useful in estimating atmospheric content given the limitations of available ground stations and the expensive costs associated with monitoring [31]. Satellite sensors provide information on a wider geographical area than ground stations, are accurate, and offer the required data that can be used in the estimation of PM concentrations in the atmosphere [32]. Subsequently, the use of satellite remote sensing has become a major source of information about the atmosphere.

Remote sensing is the science of obtaining information from a distance and is typically carried out via aircrafts or satellites. The satellites currently in orbit that provide free continuous access to AOD data are Moderate Resolution Imaging Spectroradiometer (MODIS), National Oceanic and Atmospheric Administration (NOAA), Geostationary Operational Environmental Satellite (GOES), Visible Infrared Imaging Radiometer Suite (VIIRS), and Landsat [33]. The free continuous access to such data is an essential component of a monitoring system. These types of sensors are used in obtaining atmospheric information including water and air current flow, as well as the level of pollution through estimating the levels of aerosol in the atmosphere. Operational Land Imager (OLI) and Thermal Infrared Sensor (TIRS) images are the main instruments for Landsat 8 [34]. Landsat 8 acquired multispectral bands, panchromatic band, and TIRS bands. The four optical bands of Landsat 8 used in this study have a spatial resolution of 30 m, which is sufficient for PM10 monitoring given that these particles do not propagate for long distances given their sizes [35].

Despite the numerous applications for satellite remote sensing, their use in estimating air pollutants concentrations is limited in the literature, with a few studies in which satellite images were used in prediction models for particulate matter [36–38]. Different models were developed in the literature associating spectral information from satellite imagery to the concentration of PM [39–42]. For the UAE, a country highly susceptible to sandstorms and high aerosol concentrations

due to its geography and geomorphology, satellite remote sensing can be useful in creating PM models, which would help to better understand the spatiotemporal behaviour of aerosols as they vary across the country. Only one study has attempted to create a PM10 model for the UAE, for the city of Al Ain specifically, using MODIS Aerosol Optical Depth (AOD) data to create a linear regression model correlating the AOD to the PM10 concentration over the city [43]. Developing a robust model for PM10 concentrations from Landsat imagery is needed given the frequent dust storms in the country and the region and can help not only in mapping, but also monitoring of the PM10 concentrations whenever satellite images are available.

The UAE hosts forty-one ground monitoring stations according to the Air Quality Index Manual, but this number is insufficient since it does not cover all areas, especially the remote and rural areas of the country, given that data is not accessible for most of them [44]. This study aims to monitor PM10 concentration levels covering the period 2016–2020 using Landsat 8 imagery, which will help in establishing a high-resolution remote sensing-based PM monitoring system for UAE although the temporal resolution is 16 days. This cost-effective method would complement PM10 ground monitoring techniques and provides higher spatial resolution.

The UAE is particularly susceptible to sandstorms, which increases the concentration of PM10 in the air. The UAE has also urbanized rapidly over a short period of time, especially the main cities of Abu Dhabi and Dubai, which their sizes have expanded many times their size. Therefore, it is necessary to develop a cost-effective, area-covering, air quality monitoring system that shows the pattern of the varying concentration levels of air pollutants including PM10. The main goal of this study is to develop a satellite remote sensing based PM10 monitoring system for the UAE that uses multi-spectral surface reflectance values from Landsat 8 Operational Land Image (OLI) imager, noting that such a system doesn'y currently exst and also has not been addressed in the literature for the UAE.

2 Methodology

2.1 Study area

The study area of this research is the UAE, which is a nation located in the Arabian Gulf in western Asia at the southeastern end of the Arabian Peninsula as presented in Fig. 1. Geographically, the UAE extends between 22° 50′–26° 4′ N latitudes and 51° 5′–56° 25′ E longitudes, covering a total area of 83,600 km^2, more than two-thirds of which is desert [1]. The arid/semi-arid environment of the UAE and the presence of sand and sand dunes, particularly in the southern region of the UAE and the local pollution emissions that arises from the petroleum and construction industry makes it vulnerable to

Fig. 1 Study area of the United Arab Emirates (UAE)

experience frequent sandstorms and natural dust episodes in the atmosphere, which result in increased levels of CO_2 and suspended PM [2]. One of the adverse impacts of urbanization is the increase in air pollution.

2.2 Data analysis and processing

In this section, data acquisition, including the procedures of obtaining the data from the ground monitoring stations and downloading the Landsat 8 satellite images are presented. Table 1 provides information about the characteristics of bands of Landsat 8. Landsat has a temporal resolution of 16 days, which means that the monitoring capacity is acceptable, and hence it is sufficient to capture data within the UAE [45]. Moreover, Data processing, including radiometric processing of the optical bands of Landsat 8 into reflectance values and estimating AOD, are presented. The procedure used in this study is presented in the flowchart shown in Fig. 2. Data acquisition consists of the Landsat 8 satellite images obtained for the UAE from the USGS Core Science Systems as well as obtaining PM_{10} data from ground monitoring stations. The following subsection will provide a detailed overview of the flowchart presented.

2.3 Data acquisition

Landsat 8 images were retrieved from the United States Geological Survey (USGS) Core Science Systems through the Landsat Earth Explorer [46]. The Landsat-8 payload consists of two science instruments: the Operational Land Imager (OLI) and the Thermal InfraRed Sensor (TIRS). Landsat 8 has 11 bands where nine bands are under the OLI sensor, and two bands are under the TIRS sensor [47]. Nine bands are included in the OLI instrument where bands 1–7 and band 9 are spectral bands that have 30 m spatial resolution. However, band 8 is the panchromatic band with a 15 m resolution. Moreover, the TIRS gathers the data in two long wavelength thermal infrared bands which are bands 10 and 11 that have a resolution of 100 m and are resampled to 30 m during delivery of the data product. The acquisition dates of Landsat 8 images used in the study are the years 2016, 2018, and 2020, with cloud cover of 10% or less. Also, visible bands 1, 2, 3, and 4 of Landsat 8 OLI images for the UAE area were provided within the path and row of (159–162) and (48–50), respectively.

2.4 PM10 data

PM_{10} ground measurement data in this study was obtained from the Air Pollution in World: Real-time Air Quality Index Visual Map website. The website offers daily ambient air quality monitoring data for forty-one stations in the UAE. PM_{10} data for 30 stations was used to develop the satellite remote sensing based PM_{10} model, and eleven stations were used for model validation. The literature review proved that generally dividing the testing points using the 75:25 ratio provides very good accuracy [48]. Hence, 30 stations were chosen to perform the study, which is around 75% of the existing available stations, and the other four stations were used to test the validity of the established model. Since eight satellite images are needed to capture the whole UAE domain, eight images were downloaded for each year as depicted in Fig. 3. Table 2 below shows the times at which PM10 data was used from the ground stations.

Table 1 Landsat 8 bands characteristics

Landsat 8 sensors	Band number	Band name	Wavelength (μm)	Resolution (m)
Operational land imager (OLI)	1	Coastal /Aerosol	0.43–0.45	30
	2	Blue	0.45–0.51	30
	3	Green	0.53–0.6	30
	4	Red	0.63–0.68	30
	5	Near Infrared (NIR)	0.85–0.89	30
	6	Short-wave Infrared (SWIR 1)	1.56–1.66	30
	7	Short-wave Infrared (SWIR 2)	2.10–2.30	
	8	Panchromatic	0.5–0.68	15
	9	Cirrus	1.36–1.39	30
Thermal infrared sensor (TIRS)	10	Long-wave Infrared / Thermal Infrared (TIRS 1)	10.30–11.30	100
	11	Long-wave Infrared / Thermal Infrared (TIRS 2)	11.50–12.50	100

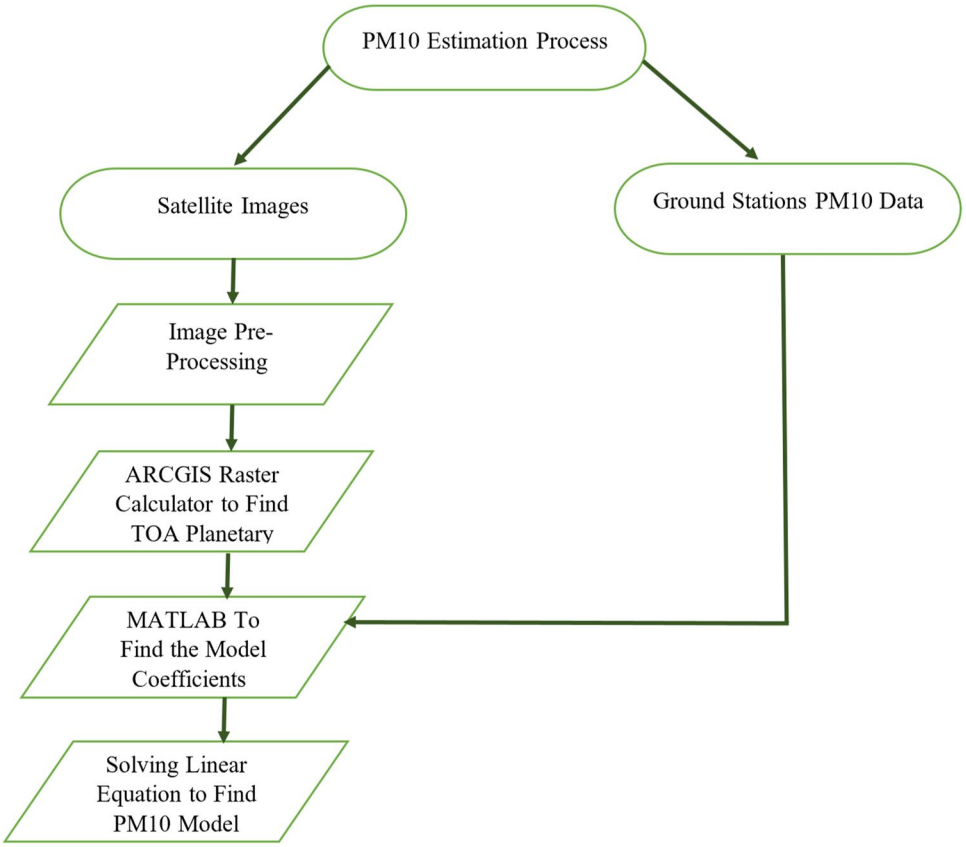

Fig. 2 Workflow Process for PM10 Estimation

2.5 Data processing

Landsat 8 Level 1 data for the four bands used in this study were first pre-corrected geometrically. Moreover, the obtained images were selected using a cloud cover mask of 10%. The data was quantified and calibrated into scaled Digital Numbers (DN) which were converted into TOA reflectance by applying radiometric correction to transform the DNs into reflectance values.

Conversion of the DNs into TOA Reflectance. The major rescaling factors in converting OLI bands data to TOA planetary reflectance (ρλ′) are independent variables consisting of band-specific multiplicative rescaling factor (M_ρ), band-specific additive rescaling factor (A_ρ), and quantized and calibrated standard product pixel values of DN (Q_{cal}). These factors were extracted from the imagery metadata files. The following equations were used to compute TOA planetary reflectance (ρλ′) following Landsat 8 standard processing methods [49].

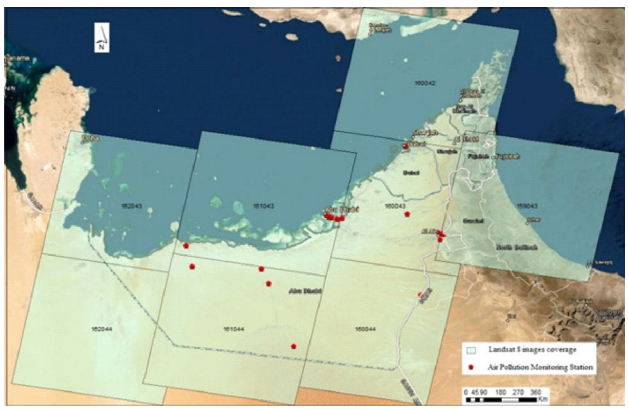

Fig. 3 PM_{10} ground monitoring stations and Landsat 8 Images covering the UAE

Table 2 Reflectance values for the four bands of each image of the selected 30 stations for the year 2016

Station	B1	B2	B3	B4
Al Muttahidia Girl School, Gayathi	0.192	0.188	0.181	0.193
Al Quaa	0.184	0.186	0.238	0.341
Al Tawia, Al Ain	0.172	0.16	0.158	0.161
Bain Al Jessrain	0.247	0.255	0.284	0.331
Dubai US Embassy	0.245	0.257	0.298	0.342
Habshan South	0.205	0.207	0.225	0.272
Islamic Institute, Al Ain	0.215	0.214	0.232	0.271
Kalifah High School, Abu Dhabi CityÂ	0.23	0.231	0.255	0.288
Khadija Primary School, Abu Dhabi City	0.155	0.137	0.133	0.124
Khalifa City	0.221	0.22	0.228	0.257
Mo'ta Girl School, Liwa Oasis	0.193	0.187	0.213	0.255
Municipality Branch office, Bida Zayed	0.22	0.227	0.277	0.352
Ruwais	0.219	0.213	0.216	0.238
School, Sweihan	0.323	0.327	0.324	0.333
US Embassy, Abu Dhabi City	0.185	0.173	0.174	0.183
akher, Al Ain	0.243	0.242	0.271	0.309
Al Ain Street	0.241	0.25	0.29	0.318
Al Mafraq	0.247	0.244	0.283	0.331
Kalba	0.218	0.218	0.231	0.266
Dibba	0.219	0.211	0.239	0.236
Al Jeer	0.218	0.229	0.248	0.301
Al Maqta	0.161	0.142	0.128	0.12
Sakamkam	0.231	0.231	0.228	0.257
Qidfaa	0.239	0.26	0.289	0.339
Al Maqta	0.233	0.23	0.228	0.283
Warsan	0.228	0.222	0.229	0.285
Nad Al Shiba	0.311	0.24	0.234	0.276
Karama	0.318	0.317	0.331	0.376
Jabeel Park	0.193	0.165	0.191	0.185
Hatta	0.252	0.235	0.266	0.317

$$\rho\lambda' = M_{\rho}Q_{cal} + A_{\rho} \tag{1}$$

Equation 1 calculates TOA reflectance without correction for solar angle and hence, Eq. 2 is used for the correction of the sun angle.

$$P\lambda = \rho\lambda\prime / \cos(\theta_{SZ}) = \rho\lambda\prime / \sin(\theta_{SE}) \tag{2}$$

where Pλ refers to TOA planetary reflectance, θ_{SE} is the local sun elevation angle, and θ_{SZ} is the local solar zenith angle. The next step involves Aerosol Optical Thickness (AOT)/AOD and PM_{10} correlation. Regression algorithm analysis is applied to correlate atmospheric AOT to PM_{10}. Aerosol Optical Thickness algorithm for a single band is represented in Eq. 3.

$$T\alpha = \left(\frac{4\mu\mu o}{\omega oPa(\theta s, \theta v, \phi}\right)\rho_{atm}(\theta_s, \theta_v, \phi). \tag{3}$$

where Τα is the AOT, ρ_{atm} is the atmospheric reflectance, θ_s is the solar zenith angle, θ_v is the viewing zenith angle, ϕ is the relative azimuth angle, μ is the cosines of view of directions, and μ_o is the cosines of the illumination directions. Similarly, AOT can be simplified, and Eq. 3 can be simplified into Eq. 4 with the addition of different constants.

$$AOT(\lambda) = a_oR\,\lambda_1 + a_1R\lambda_2 + a_2R\lambda_3 + a_3R\lambda_4 \tag{4}$$

Table 3 Model coefficients obtained based on the equations

Model coefficients	Calculated value
a0	2480.5
a1	1330.3
a2	2618.8
a3	1653.4

where $R\lambda_1$, $R\lambda_2$, $R\lambda_3$, and $R\lambda_4$, are the reflectance that correspond to bands 1, 2, 3, and 4 of Landsat 8 respectively. While the a_j are the model coefficients that are empirically determined. The relationship between AOT and PM_{10} is established using a single and homogenous atmospheric layer that contains spherical aerosol particles. Therefore, the particulate matter concentration can be compared significantly with the AOT directly to determine air pollution. Different software systems were used in this study to complete the processing and the model development. The ESRI ® ArcGIS was utilized to calculate the TOA reflectance values using Eq. 2. The band-specific multiplicative rescaling factor (M_ρ), band-specific additive rescaling factor (A_ρ), quantized and calibrated standard product pixel values of DN (Q_{cal}) and the local sun

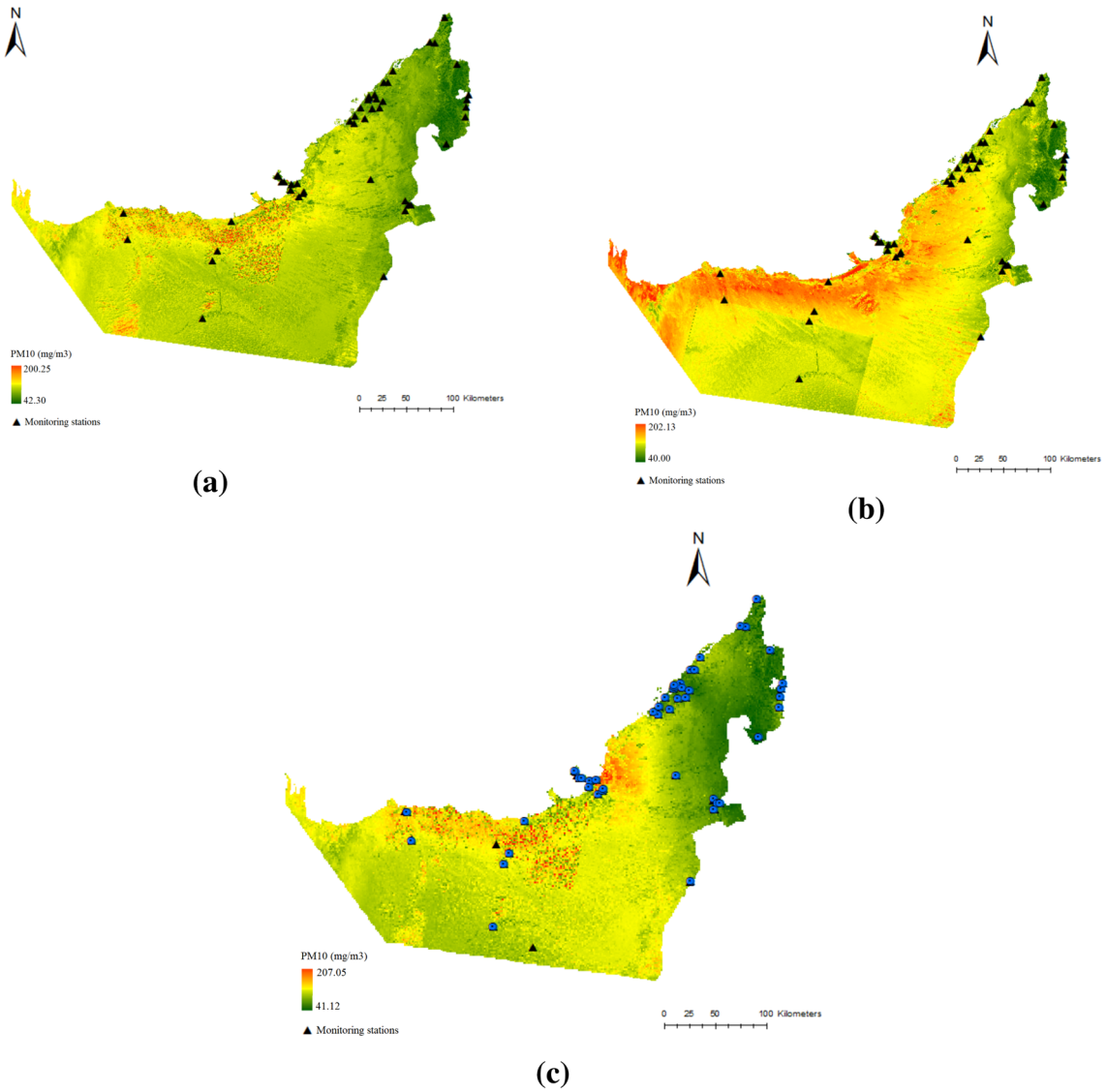

Fig. 4 **A** PM_{10} concentration in a color-coded image covering the whole UAE in December 2017. **B** PM_{10} concentration in a color-coded image covering the whole UAE in September 2019. **C** PM_{10} concentration in a color-coded image covering the whole UAE in September 2021

elevation angle (θ_{SE}) were extracted from the MTL Notepad files that come with the images in order to proceed with the reflectance TOA calculations.

Out of the existing forty-one ground monitoring stations in the UAE, only sixteen stations have accessible PM_{10} data, as mentioned earlier. Table 2 shows the sixteen stations that are used in this study. Data from twelve of these stations were used to develop the model coefficients (a_o, a_1, a_2 and a_3) which are shown in Eq. 4. Normally, PM10 can be determined as a function of AOT by incorporating Eq. 4 into Eq. 5 [50] and [51].

$$PM_{10} = a_oB_1 + a_1B_2 + a_2B_3 + a_3B_4 \quad (5)$$

where B_1, B_2, B_3, and B_4 are the reflectance values calculated using Eq. 2 in ArcGIS raster calculator. The values a_o, a_1, a_2, and a_3 are the model coefficients that were calculated using MATLAB in order to solve the PM_{10} linear equations. Considering the twelve stations by adopting the data of the three selected years resulted in establishing a system of thirty-six linear equations that were solved in MATLAB using the minimum mean square error method to resolve the indeterminate situation.

3 Results and discussion

In this section, the resulting values and coefficients to establish the PM_{10} monitoring model are presented. Moreover, the model was stablished and validated to determine the PM_{10} concentration for any location within the UAE. Table 2 shows the reflectance values for the four bands of each image of the selected twelve stations for the year 2016 and similar calculations were performed for years 2018, 2020, and 2022.

Using data from 30 ground stations, 120 equations were established. The minimum mean square error method in MATLAB was used to estimate the model coefficients (a_o, a_1, a_2, and a_3), which are shown in Table 3. The finalized spectral model is shown in Eq. 6.

$$PM_{10} = 2480.5B_1 + 1330.3B_2 + 2618.8B_3 + 1653.4B_4 \quad (6)$$

As mentioned earlier, data from 30 stations were used to establish the model. The remaining 11 stations were used for validation. The model R-squared (R^2) value was estimated to be around 65%. This value indicates that the model can robustly estimate the PM_{10} concentrations spectrally, given Landsat 8 availability at the location of interest.

In comparison to previous studies, our model R^2 value is lower than that obtained by [52] for Delhi, India and by [53] over Kirkuk, Iraq. These studies reported R^2 values of 80% and 83%, respectively. The reason for obtaining a lower R^2 value for our spectral model is the use of time series data for 2016, 2018, and 2020, respectively. This is an advantage to our model, which takes into consideration the atmospheric variations over the period of study, unlike the previous studies that were conducted over one episode of time. This time consideration is advantageous to our study and definitely has a huge impact on the variability of PM_{10} concentrations due to many factors. This demonstrates the uniqueness of our model, which reflects the spatial and temporal variation of atmospheric factors such as wind speed, direction, humidity, and atmospheric pressure. In addition to the R^2 assessment, Root Mean Square Error is another accuracy measure that shows the robustness of the model. RMSE was calculated for the model and found to be 17.67 μg/m^3. Further, data from eleven ground stations were used for model validation. The result revealed a satisfactory R^2 value of 82.15% with a RMSE of 16.88 μg/m^3.

The model has demonstrated robustness in estimating PM_{10} concentrations from the four bands of Landsat 8 imagery, Landsat images were downloaded for December 2017, September 2019, and December 2021 to represent different seasons of the year. Landsat images were processed and mosaiced for the purpose of visualizing PM_{10} concentration, which are estimated with the spectral model in color-coded maps covering the UAE. Figure 4 shows the color-coded images for December 2017, September 2019, and December 2021 images.

It can be inferred from Fig. 4that the red areas represent high PM_{10} concentration, yellow areas represent a medium concentration, and the green areas represent a low PM_{10} concentration area. Although the month of September is normally not windy, PM_{10} levels were still higher than in December 2017. This increase in the particulate matter concentration is due to the urbanization expansion and the related increased level of air pollution. The study also confirmed that the time of the year has a huge impact in particulate matter concentration. Furthermore, high levels of PM are observed during the dusty summer season as a result of the Shamal winds, which is known for producing notable sandstorms. In fact, the PM concentration is linked to the emissions of the primary and the secondary PM initiators, including natural

atmospheric causes such as the Shamal winds [54]. The color-coded map of December 2017 (Winter season) shows less PM_{10} concentration than that estimated in September 2019 (End of the summer season), taking into consideration the increase in the urbanization and pollution rates over the years from 2017 to 2019.

4 Conclusion

This study aimed at developing a remote sensing-based model for estimating and monitoring of PM10 levels in the UAE. Given that PM_{10} is a major contributor to air pollution and has adverse health effects, this study has attempted to develop a spectral model based on Landsat 8 data. The model R-squared value of 65% and the Root Mean Square Error (RMSE) of 12.55 µg/m3 show the model efficiency. The results of the study have demonstrated the successful use of Landsat 8 imagery in estimating PM_{10} concentration over the UAE. The resulting spectral model, which has a monitoring potential, can be used to estimate PM_{10} values at any location in the UAE where Landsat 8 data is available. The results of the study are in agreement with that of [33] and [34]. Moreover, ArcGIS and MATLAB software systems were essential in the process to ease the set of calculations in order to obtain the model and complete this study. Furthermore, the results proved that satellite imagery could be used in monitoring PM_{10} over large areas.

Although the results of the study showed that the model is robust in estimating PM_{10} concentration in UAE, the model would have been more robust if the data of all the existing ground monitoring stations were accessible. Using more ground monitoring stations in future studies will improve the results, and therefore the model will be improved. Furthermore, studying the contribution of the seasonal variations and the geographical locations of the PM_{10} concentrations, and the variation in related atmospheric factors would help in understanding the causes of high PM_{10} concentration variability over time.

Author contributions "Conceptualization, T. Ali M. Singer and A. Al Suwaidi; methodology, T. Ali, S. Atabay and A. Elaksher; software, A. Al Suwaidi and S. Atabay.; validation, T. Ali and A. Elaksher; formal analysis, A. Elaksher and M. Singer; investigation, T. Ali and. Al Suwaidi; writing—original draft preparation, T. Ali and. Al Suwaidi; writing—review and editing, A. Elaksher,S. Atabay and M. Singer. All authors have read and agreed to the published version of the manuscript."

Funding Not applicable.

Availability of data and material Landsat the statements, opinions and data contained in all publications are solely those of the individual author(s) and contributor(s).

Declarations

Competing interests Not applicable.

References

1. Abdelfattah M, Shahid S, Othman Y. Soil salinity mapping model developed using RS and GIS—a case study from Abu Dhabi, United Arab Emirates. Eur J Sci Res. 2009;26:342–51.
2. Abuelgasim A, Farahat A. Effect of dust loadings, meteorological conditions, and local emissions on aerosol mixing and loading variability over highly urbanized semiarid countries: United Arab Emirates case study. J Atmos Solar Terr Phys. 2020;199:105215. https://doi.org/10.1016/j.jastp.2020.105215.
3. Acharya T, Yang I. Exploring Landsat 8. Int J IT Eng Appl Sci Re. 2015;4:4–10.
4. Al-Taani AA, Nazzal Y, Howari FM, Yousef A. Long-term trends in ambient fine particulate matter from 1980 to 2016 in United Arab Emirates. Environ Monit Assess. 2019;191(3):143. https://doi.org/10.1007/s10661-019-7259-9.
5. Amoatey P, Omidvarborna H, Baawain M, Al-Mamun MdA. Indoor air pollution and exposure assessment of the gulf cooperation council countries: a critical review. Environ Int. 2018. https://doi.org/10.1016/j.envint.2018.09.043.

6. Chen J, Huang X. Estimating hourly PM2.5 concentrations from himawari-8 AOD over Hubei province. 2018. Int Archiv Photogramm Remote Sens Spatial Inform Sci. https://doi.org/10.5194/isprs-archives-XLII-4-77-2018.
7. Fang C, Liu H, Li G, Sun D, Miao Z. Estimating the impact of urbanization on air quality in China using spatial regression models. Sustainability. 2015;7(11):15570–92.
8. Bai Y, Wu L, Qin K, Zhang Y, Shen Y, Zhou Y. A geographically and temporally weighted regression model for ground-level pm2.5 estimation from satellite-derived 500 m resolution AOD. Remote Sens. 2016;8(3):262. https://doi.org/10.3390/rs8030262.
9. Bhagavathula A, Shehab A. Ambient air pollution: a major modifiable cardiovascular risk factor in the UAE? J Cardiovasc Dis Res. 2019;10:99–99. https://doi.org/10.5530/jcdr.2019.3.20.
10. Ghorani-Azam A, Riahi-Zanjani B, Balali-Mood M. Effects of air pollution on human health and practical measures for prevention in Iran. J Res Med Sci. 2016;21:65. https://doi.org/10.4103/1735-1995.189646.
11. Guo H, Cheng T, Gu X, Chen H, Wang Y, Zheng F, Xiang K. Comparison of four ground-level PM2.5 estimation models using PARASOL aerosol optical depth data from China. Int J Environ Res Publ Health. 2016;13(2):180. https://doi.org/10.3390/ijerph13020180.
12. Hadjimitsis DG. Aerosol optical thickness (AOT) retrieval over land using satellite image-based algorithm. Air Qual Atmos Health. 2009;2(2):89–97. https://doi.org/10.1007/s11869-009-0036-0.
13. Hadley MB, Baumgartner J, Vedanthan R. Developing a clinical approach to air pollution and cardiovascular health. Circulation. 2018;137(7):725–42.
14. Holben BN, Tanré D, Smirnov A, Eck TF, Slutsker I, Abuhassan N, et al. An emerging ground-based aerosol climatology: aerosol optical depth from AERONET. J Geophys Res Atmospheres. 2001;106(D11):12067–97. https://doi.org/10.1029/2001JD900014.
15. Hrdličková Z, Michálek J, Kolář M, Veselý V. Identification of factors affecting air pollution by dust aerosol PM10 in Brno City. Czech Republ Atmospheric Environ. 2008;42(37):8661–73. https://doi.org/10.1016/j.atmosenv.2008.08.017.
16. Heft-Neal S, Burney J, Bendavid E, Burke M. Robust relationship between air quality and infant mortality in Africa. Nature. 2018;559(7713):254–8. https://doi.org/10.1038/s41586-018-0263-3.
17. Hu K, Davison T, Rahman A, Sivaraman V. Air pollution exposure estimation and finding association with human activity using wearable sensor network. In Proceedings of the MLSDA 2014 2nd workshop on machine learning for sensory data analysis—MLSDA'14. Gold Coast: ACM Press; 2014. p. 48–55.
18. Jacobson MZ. Review of solutions to global warming, air pollution, and energy security. Energy Environ Sci. 2009;2(2):148–73. https://doi.org/10.1039/B809990C.
19. Jassim MS, Coskuner G, Zaid M, Malik U. Analysis of aerosol optical depth over Bahrain and eastern province of Saudi Arabia based on MERRA-2 model. Int J Environ Sci Technol. 2020;19(2):863–74. https://doi.org/10.1007/s13762-020-02987-4.
20. Kalajdjieski J, Zdravevski E, Corizzo R, Lameski P, Kalajdziski S, Pires IM, et al. Air pollution prediction with multi-modal data and deep neural networks. Remote Sensing. 2020;12(24):4142.
21. Kamarul Zaman NAF, Kanniah KD, Kaskaoutis DG. Estimating Particulate matter using satellite based aerosol optical depth and meteorological variables in Malaysia. Atmos Res. 2017;193:142–62. https://doi.org/10.1016/j.atmosres.2017.04.019.
22. Air Quality in United Arab Emirates, IQAIR, https://www.iqair.com/united-arab-emirates. Accessed 06 July 2023.
23. Landsat 8, Landsat Missions, USGS. https://www.usgs.gov/landsat-missions/landsat-8. Accessed 06 Sep 2023.
24. Sentintel-5P, The European Space Agency, https://sentinels.copernicus.eu/web/sentinel/missions/sentinel-5p. Accessed 06 July 2023.
25. UAE weather: Beware! There's a sandstorm in the UAE, Gulf News, https://gulfnews.com/uae/weather/uae-weather-beware-theres-a-sandstorm-in-the-uae-1.1595331530584?slide=1. Accessed 06 Sep 2023.
26. Ke Y, Im J, Lee J, Gong H, Ryu Y. Characteristics of Landsat 8 OLI-derived NDVI by comparison with multiple satellite sensors and in-situ observations. Remote Sens Environ. 2015;164:298–313. https://doi.org/10.1016/j.rse.2015.04.004.
27. Kokkalis PK, Aljassar H, Solomos S, Raptis P-I, Alhendi H, Amiridis V, et al. Long-term ground-based measurements of aerosol optical depth over Kuwait City. Remote Sens. 2018;10(11):1807. https://doi.org/10.3390/rs10111807.
28. Liu Y, Zhao J, Deng R, Liang Y, Gao Y, Chen Q, et al. A downscaled bathymetric mapping approach combining multitemporal Landsat-8 and high spatial resolution imagery: demonstrations from clear to turbid waters. ISPRS J Photogramm Remote Sens. 2021;180:65–81. https://doi.org/10.1016/j.isprsjprs.2021.07.015.
29. Manisalidis I, Stavropoulou E, Stavropoulos A, Bezirtzoglou E. Environmental and health impacts of air pollution: a review. Front Public Health. 2020. https://doi.org/10.3389/fpubh.2020.00014.
30. Mohamed G. Estimation of PM10 concentration using ground measurements and Landsat 8 OLI satellite image. J Appl Remote Sens. 2014;3(2):2169.
31. Al Yammahi A, Aung Z. Forecasting the concentration of NO2 using statistical and machine learning methods: A case study in the UAE. Heliyon. 2023;9(2):E12584.
32. El Kenawy AM, Lopez-Moreno JI, McCabe MF, Dominguez-Castro F, Pena-Angulo D, Gaber IM, Alqasemi AS, Al Kindi KM, Al-Awadhi T, Hereher ME, Robaa SM, Al Nasiri N, Vicente-Serrano SM. The impact of COVID-19 lockdowns on surface urban heat island changes and air-quality improvements across 21 major cities in the Middle East. Environ Pollut. 2021;288:117802.
33. Saraswat I, Mishra RK, Kumar A. Estimation of PM10 concentration from Landsat 8 OLI satellite imagery over Delhi, India. Remote Sens Appl Soc Environ. 2017;8:251–7.
34. Saleous N, Issa S, Alsuwaidi M. Using Modis aerosol optical depth to predict PM10 over Al Ain Region, UAE. In: The international archives of the photogrammetry, remote sensing and spatial information sciences, Volume XLIII-B3–2021 XXIV ISPRS Congress. ISPRS, Hannover. 2021. 419–423
35. Wang J, Christopher SA. Intercomparison between satellite-derived aerosol optical thickness and PM2.5 mass: Implications for air quality studies. Atmospheric Sci. 2003;30(21).
36. Mulrennan K, Donovan J, Tormey D, Macpherson R. A data science approach to modelling a manufacturing facility's electrical energy profile from plant production data. In 2018 IEEE 5th International Conference on Data Science and Advanced Analytics (DSAA). 2018;387–391. https://doi.org/10.1109/DSAA.2018.00050.
37. Omari K, Abuelgasim A, Alhebsi K. Aerosol optical depth retrieval over the city of Abu Dhabi, United Arab Emirates (UAE) using Landsat-8 OLI images. Atmos Pollut Res. 2019;10(4):1075–83. https://doi.org/10.1016/j.apr.2019.01.015.

38. Ostro BD, Tran H, Levy JI. The health benefits of reduced tropospheric ozone in California. J Air Waste Manag Assoc. 2006;56(7):1007–21.
39. Pope CA III, Dockery DW. Health effects of fine particulate air pollution: lines that connect. J Air Waste Manag Assoc. 2006;56(6):709–42.
40. Rabha S, Saikia BK. (2020). 18—Advanced micro- and nanoscale characterization techniques for carbonaceous aerosols. In: C. Mustansar Hussain (Eds). Handbook of Nanomaterials in Analytical Chemistry. Amsterdam: Elsevier. 449–472. https://doi.org/10.1016/B978-0-12-816699-4.00018-9.
41. Roy DP, Wulder MA, Loveland TR, Allen RG, Anderson MC, et al. Landsat-8: science and product vision for terrestrial global change research. Remote Sens Environ. 2014;145:154–72. https://doi.org/10.1016/j.rse.2014.02.001.
42. Othman N, Mat Jafri MZ, Lim HS, Abdullah K. Satellite retrieval of aerosol optical thickness over arid region: case study over Makkah, mina and Arafah, Saudi Arabia. J Appl Sci. 2010;10:3021–31.
43. UAE Air Quality Index Manual, MOCCAE, https://www.moccae.gov.ae/assets/91c95f18/uae-air-quality-index-manual.aspx. Accessed 06 July 2023.
44. Abuelgasim A, Farahat A. Investigations on PM10, PM2.5, and Their ratio over the emirate of Abu Dhabi, United Arab Emirates. Earth Syst Environ. 2020;4:763–75.
45. Heimhuber V, Tulbure MG, Broich M. Addressing spatio-temporal resolution constraints in Landsat and MODIS-based mapping of large-scale floodplain inundation dynamics. Remote Sens Environ. 2018;211:307–20.
46. Saleh SAH, Hasan G. Estimation of PM10 concentration using ground measurements and Landsat 8 OLI satellite image. J Geophys Remote Sens. 2014;3(2):2169.
47. Saraswat I, Mishra RK, Kumar A. Estimation of PM10 concentration from Landsat 8 OLI satellite imagery over Delhi, India. Remote Sens Appl Soc Environ. 2017;8:251–7. https://doi.org/10.1016/j.rsase.2017.10.006.
48. Ung A, Weber C, Perron G, Hirsch J, Kleinpeter J, Wald L, Ranchin T. Air pollution mapping over a city—virtual stations and morphological indicators. 2001. https://hal-mines-paristech.archives-ouvertes.fr/hal-00465566. Accessed 18 July 2022.
49. Zhang K, de Leeuw G, Yang Z, Chen X, Su X, Jiao J. Estimating Spatio-temporal variations of PM2.5 concentrations using VIIRS-derived AOD in the Guanzhong basin China. Remote Sens. 2019;11(22):2679. https://doi.org/10.3390/rs11222679.
50. Zhang Y, Jiang W. Pollution characteristics and influencing factors of atmospheric particulate matter (PM2.5) in Chang-Zhu-Tan area. IOP Conf Earth Environ Sci. 2018;108:042047. https://doi.org/10.1088/1755-1315/108/4/042047.
51. Powerful sandstorm and rain strike Abu Dhabi, The National, https://www.thenationalnews.com/uae/environment/powerful-sandstorm-and-rain-strike-abu-dhabi-1.1053200. Accessed 06 Jun 2023.
52. Kaied YO, Darwish ASK, Farrell P. COVID-19 impact on air quality and associated elements: knowledge data of the Emirate of Ajman—UAE. Renew Energy Environ Sustain. 2021. https://doi.org/10.1051/rees/2021010.
53. Zhang C, Li J, Zhao W, Yao Q, Wang H, Wang B. Open biomass burning emissions and their contribution to ambient formaldehyde in Guangdong province. China Sci Total Environ. 2022;838(1):155904.
54. Qiu S, He Z, Liu G, Ding Z, Bu Z, Cao J, Ji W, Liu W, Su C, Wang X, Liu F, Li F, Li T, Qian H, Liu C. Ambient formaldehyde concentrations in summer in 30 Chinese cities and impacts on air cleaning of built environment. Energy Built Environ. 2023. https://doi.org/10.1016/j.enbenv.2023.03.003.